INTERNATIONAL JOURNAL OF
RADIATION ONCOLOGY • BIOLOGY • PHYSICS
www.redjournal.org

BIOLOGY CONTRIBUTION

Diffusing Alpha-Emitters Radiation Therapy Promotes a Proimmunogenic Tumor Microenvironment and Synergizes With Programmed Cell Death Protein 1 Blockade

Sara Del Mare, PhD,* Yossi Nishri, PhD,* Amit Shai, MSc,* Margalit Efrati, MSc,* Lisa Deutsch, PhD,† Robert B. Den, MD,*,‡ Itzhak Kelson, PhD,§ Yona Keisari, PhD,‖ and Vered Domankevich, PhD*

*Translational Research Laboratory, Alpha Tau Medical Ltd., Jerusalem, Israel; †BioStats Statistical Consulting Ltd., Maccabim, Israel; ‡Radiation Oncology, Thomas Jefferson University, Philadelphia, Pennsylvania, USA; §Sackler Faculty of Exact Sciences, School of Physics and Astronomy, Tel Aviv University, Tel Aviv, Israel; and ‖Clinical Microbiology and Immunology, Sackler Faculty of Medicine, Tel Aviv University, Tel Aviv, Israel

Received Jun 27, 2022; Accepted for publication Aug 18, 2022

Purpose: Diffusing alpha-emitters Radiation Therapy (DaRT) releases alpha-emitting atoms into the tumor microenvironment. The treatment effectively ablates human and mice xenografts and shows 100% response rates in skin or head and neck squamous cell carcinoma patients. DaRT induces specific and systemic antitumor immune activation and synergizes with immune stimulation and modulation in mice. Here, the transcriptional profile activated by DaRT, and its potential to enhance responsiveness to immune checkpoint inhibition by programmed cell death protein 1 (PD-1) blockade were studied.

Methods and Materials: Squamous cell carcinoma tumor- bearing BALB/C mice were treated with DaRT or inert seeds in combination with anti-PD-1 (aPD-1) or IgG control antibody. Sixteen days after seed insertion, tumors and spleens were subjected to immunophenotyping and immunohistochemical staining. Combination of DaRT and aPD-1 was tested for efficacy. Gene expression analysis was performed on mRNA extracted from tumors 7 days after DaRT or inert insertion using Nanostring PanCancer-IO-360 panel, and tumors and spleens were subjected to flow cytometry analysis.

Results: DaRT in combination with aPD-1 delayed tumor development, induced CD3 and CD8 lymphocytes infiltration more efficiently than either monotherapy. The combined treatment reduced splenic polymorphonuclear myeloid derived suppressor cells more than aPD-1 therapy or control. Granzyme B release in the tumor was increased only in the combinational treatment and was correlated with T-lymphocyte infiltration. Gene expression and gene set enrichment analysis of mRNA levels 7 days after DaRT insertion indicated that DaRT upregulated apoptosis, p53 signaling, G1/S-related arrest, interferon signaling and

Corresponding author: Vered Domankevich, PhD; E-mail: veredb@alphatau.com

All support for the present manuscript, included materials and reagents were funded by Alpha Tau Medical LTD, Jerusalem, Israel.

Disclosures: Y.K., I.K., and L.D. are consultants of Alpha Tau Medical; Y.K. is also a member of the International Cancer Microenvironment Society and of the Scientific committee MOST-DKFZ grants; R.B.D. is the Chief Medical Officer of Alpha Tau Medical; Y.K., I.K, V.D., M.E., S.D., A.S., Y.N., and L.D. hold stock options of Alpha Tau Medical; Y.N., M.E., A.S., S.D., and V.D. are employees in Alpha Tau Medical; Y.K., I.K., V.D., S.D., Y.N., R.B.D., M.E., and A.S. are the authors of a patent application related to this study. L.D. is the CEO of BioStats Statistical Consulting.

Data Sharing Statement: Research data are stored in an institutional repository and will be shared upon request to the corresponding author.

Acknowledgments—We thank Prof Michal Lotem, Drs Galit Eisenberg, Eilam Yeini, Assaf Malik, Michael Mintz, and Sharon Grisaru for their valuable advice. We thank Drs Daria Makarovsky and Orit Sagi-Assif from the Tel Aviv university core facility, Drs Liat Linde from Technion core facility and Haifa Aqeilan from Hadassah medical center pathology facility, and Dr Michael Harlev from Tel-Aviv University animal facility, for their assistance and support.

Supplementary material associated with this article can be found in the online version at doi:10.1016/j.ijrobp.2022.08.043.

https://doi.org/10.1016/j.ijrobp.2022.08.043

myeloid related transcription, while downregulating DNA repair, cell proliferation, and notch-related transcription. Flow cytometry showed that DaRT increased dendritic cells activation and led to changes in MDSCs distribution.

Conclusions: DaRT promotes a "hot" tumor microenvironment and changes in immune suppression that lead to a potentiation of aPD-1 blockade induced effector T cell function and improved treatment efficacy. This study provides rationale for investigating DaRT and aPD-1 combination in patients with squamous cell carcinoma.

Introduction

Cancer immunotherapy aims to enhance and restore antitumor effector immune cell functions[1,2] by targeting a variety of suppressive pathways. The most common strategy is immune checkpoint blockade-based therapy that uses programmed cell death protein/ligand 1 (PD-1/PDL-1) antibodies, which block the signaling that inhibits T cell activation.[3] Despite the wide clinical usage of anti-PD-1/PD-L1 therapies, those treatments showed therapeutic efficacy only in a subset of patients and a high percentage of the initial responders eventually develop resistance.[4] Preclinical and clinical studies have been conducted using anti-PD-1 (aPD-1) in combination with other treatment modalities.[5] These include local therapies such as oncolytic viruses or tumor ablation, for example by radiation therapy (RT), that were used to activate a systemic antitumor immune response, which may synergize with immune checkpoint blockade.[6]

RT is known to stimulate an immune response by releasing tumor antigens and damage associated molecular patterns molecules (DAMPs), which may attract and activate antigen presenting cells (APCs).[7] In addition, the damage induced by radiation may cause the stimulation of interferon genes (STING) pathways, by the release of double-strand DNA to the cytosol[8] and the activation of type I interferon response, which leads to PD-L1 upregulation.[9] Thus, combining immune checkpoint inhibitors that target PD-1/PD-L1 with radiation might protect T cells from anergy and apoptosis and potentiate the antitumor response.[10] Numerous preclinical studies showed an improved efficacy of aPD-1/aPD-L1 checkpoint therapy combined with different RT modalities[11-14] and abscopal effects have been increasingly reported in patients treated with the combination.[15] Combination therapies were associated with higher infiltration and enhanced activation of CD8+ T cells, upregulation of PD-L1 and MHC class I/tumor antigens complexes with the consequent enhancement of antigen cross-presentation.[16] However, RT may also negatively affect immune organs such as bone marrow,[17] and the optimal RT type and treatment sequence is still under investigation.

Diffusing alpha-emitters Radiation Therapy (DaRT) is a unique RT modality that was recently shown to induce effective tumor responses in patients with head and neck and skin squamous cell carcinoma (SCC), leading to 100% response rates, among them 78.6% complete response,[18] including a case report that demonstrated abscopal responses.[19] DaRT uses ^{224}Ra ($t_{½}$ = 3.63 days) loaded sources that continuously release alpha-emitting atoms into the tumor tissue, such that 95% of the total dose is delivered within 16 days. For a seed carrying a few μCi of ^{224}Ra, therapeutically relevant alpha particle dose (>10 Gy per seed) is delivered within a diameter of 3 to 5 mm.[20,21] Alpha radiation is a type of high linear energy transfer (LET) radiation, which is characterized by higher biological efficiency[22,23] due to the creation of clustered DSBs in the DNA, which are almost impossible to repair.[23-26] In addition, the short killing range provides a high safety profile that spares the adjacent tissues and organs.[27] In preclinical studies, DaRT induced an immune memory in CT26 treated mice that became resistant to tumor rechallenge in the lungs and skin.[28] DaRT seed mediated tumor growth retardation was increased by T regulatory cells (Tregs) inhibition and myeloid derived suppressor cells (MDSCs) function suppression.[29] Moreover, DaRT in combination with CpG and Tregs/MDSCs inhibitors led to 51% tumor elimination, whereas each monotherapy led mostly to tumor recurrence. These cured mice were resistant specifically to CT26 rechallenge and their splenocytes mediated tumor cell specific resistance in naïve mice.[30] In addition, local cytoplasmatic delivery of polyIC in combination with DaRT synergistically retarded tumor growth, reduced lung metastases load, and prolong metastases related survival in the 4T1 mice model of triple negative breast cancer.[31]

DaRT was not tested yet in combination with aPD-1, which is the focus of the current study. The clinical motivation for investigating the combination between DaRT and aPD-1 treatments would be the potential increase of complete remission (CR) rates in DaRT treated patients and the prevention of local recurrence. In addition, the potential increase in the responsiveness to aPD-1, due to systemic antitumor immune activation may increase abscopal responses. In the current study we investigated the effect of DaRT in combination with aPD-1 checkpoint inhibitor on tumor growth in the murine SCC tumor model SQ2 and characterized the immunologic events taking place in response to DaRT at an early time point or to the combination at the end of the treatments. In addition, gene expression in response to DaRT treatment provided insight to underlying mechanisms.

Methods and Materials

Animals

This study does not involve human subjects. All animal experiments were carried out in accordance with the government and institution guidelines and regulations (ethical request approval 01-20-097) and with the National Institutes of Health guide for the care and use of laboratory animals (National Institutes of Health Publications No. 8023, revised 1978). BALB/c male mice (17.5 weeks old, 28 g body weight) were obtained from Envigo (Jerusalem, Israel) and were kept in the animal facility of Tel Aviv University. All surgical and invasive procedures were performed under anesthesia using ketamine (100 mg/kg, Bremer Pharma, Germany) and xylazine hydrochloride (10 mg/kg, Eurovet Animal Health B. V., Bladel, Netherlands) solution in PBS.

Cell lines

SQ2 murine squamous cell carcinoma (kindly provided by Dr. Gad Lavie from the Sheba Medical Center, Tel HaShomer, Israel)[32] were grown in Dulbecco's modified eagle medium supplemented with 10% fetal calf serum, penicillin (100 U/mL), streptomycin (100 μg/mL), and nystatin (12.5 U/mL; Biological Industries, Kibbutz Beit Haemek, Israel). Cells were incubated in a humid incubator at a temperature of 37°C and 5% CO_2.

Tumor cell inoculation

SQ2 tumor cells were inoculated at a concentration of 5×10^5 cells/50 μl in Hanks' balanced salt solution (HBSS, Biological Industries, Kibbutz Beit Haemek, Israel). Mice were inoculated intracutaneously into the right low lateral side of the back.

^{224}Ra-loaded seed preparation and insertion

Stainless steel (316 LVM) 0.7 mm diameter tubes in the length of 6.5 mm were loaded with ^{224}Ra atoms seed, after an electrostatic collection process similar to that previously described.[21] To prevent radium detachment from the surface, the seeds were coated with a 1 mm polymeric layer (Nusil, med2-4213 model). The ^{220}Rn desorption probability (the probability that a ^{220}Rn atom is emitted from the seed following a decay of ^{224}Ra) was ~45% and the ^{224}Ra activity per seed was 75 kBq, unless mentioned otherwise. Seeds, either loaded with ^{224}Ra or inert, were placed near the tip of a 19-gauge needle, which is attached to an insertion applicator. The radioactive and inert seeds were inserted into the tumor mass under anesthesia. The seeds are not removed from the tumor along the experiment.

In vivo tumor measurements and exclusion criteria

Local tumor growth was determined by measuring 3 mutually orthogonal tumor dimensions 2 to 3 times per week, according to the following formula: Tumor volume = $\pi/6 \times$ Diameter 1 $\times$ Diameter 2 $\times$ Height. Daily survival monitoring was performed and recorded. Mice were excluded across the different groups due to the presence of double tumors or due to unexpected death probably due to fight wounds.

Anti PD-1 treatment

Rat antimouse PD-1 (BE00146, BioxCell) was dissolved in InVivoPure antibody dilution buffer pH = 7 (IP0070, BioxCell). Isotype control InVivoMAb Rat IgG2a (BE0089, BioxCell) was dissolved in InVivoPure isotype dilution buffer pH = 6.5, (IP0065, BioxCell). 10 mg/kg aPD-1 or isotype control (IgG) were given intraperitoneally in a volume of 200 μl.

Flow cytometry analysis

Flow cytometry analysis was performed on freshly isolated cells from spleens and tumors. Mice were sacrificed, and spleens and tumors were collected in ice-cold PBS. Tumors were enzymatically dissociated with Collagenase (1.5 mg/mL), Hyaluronidase (0.75 mg/mL), and DNase (0.1 mg/mL), and splenocytes were collected by mashing the spleen through a 70 μM cell strainer and red blood cell lysis was done with Ack lysis buffer (0.15M NH_4Cl, 0.01 M $KHCO_3$, and 0.1 mM Na_2EDTA). For flow cytometry staining, the single cell suspensions were incubated with anti-CD16/32 (Mouse BD Fc Block, BD Biosciences) to block Fc receptors (FcRs) for 5 min at 4°C and stained for 30 minutes at 4°C with the following antibodies mixture: CD11c-PE-cy7, CD86-BV650, CD45-APC, MHC Class II-PE, CD11b-BB515, Ly6G-BV421, and Ly6C-PE-CF594. After 2 washes in flow cytometry analysis Buffer (PBS + 2% fetal bovine serum + 5 mM EDTA), samples were read in the S1000EXi Flow cytometry instrument (Stratedigm, CA). Dendritic cells (DCs) were identified as CD45+, CD11c, and MHC-II double positive cells. CD86 was used as an activation marker. MDSCs were identified as CD45+, CD11b+ Ly6G+ $Ly6C^{low}$ polymorphonuclear myeloid derived suppressor cells (PMN-MDSC) or CD45+, CD11b+ $Ly6G^{-}Ly6C^{high}$ mononucleated myeloid suppressor cells (M-MDSC). FlowJo v.10 software was used to analyze the immune populations using the gating strategy described in Fig. S1.

Immunohistochemistry

Tumor specimens were cut in 5 μm sections from O.C.T. embedded frozen blocks. Slides were fixed in cold acetone for 20 minutes and then washed in PBS. Staining was

performed with a Leica Bond-III Automated Stainer (Leica Biosystems, Germany). Blocking was done with 5% Normal Goat Serum (NGS), 5% Bovine Serum Albumin (BSA) in PBS for 1 hour. Primary antibodies used were Rabbit antimouse CD3 (abcam AB-ab16669) 1:400, Rabbit antimouse CD8 alpha (abcam ab217344) 1:500, Rabbit antimouse Ggranzyme B (abcam ab255598) 1:200, Rabbit antimouse Foxp3 (abcam ab215206) 1:500 diluted in Blocking Solution. Primary antibodies were incubated for 60 minutes, followed by detection using the BOND Polymer Refine HRP Plex Detection Kit (DS9914, Leica Biosystems, Germany) for 15 minutes. Nuclei were subsequently visualized with Hematoxylin, and the section was coverslipped using Micromount mounting medium (3801730, Leica Biosystems, Germany). Immunostained slides were scanned using the Aperio VERSA Slide Scanner (Leica Biosystems, Germany) at a 20 × magnification. The expression of CD3+, CD8+, GrmB +, and Foxp3+ cells was analyzed in the tumor center (TC), approximately 250 μm from the margin, excluding necrotic areas. At least 3 representative regions of interest were drawn in the QuPath software and the number of positive cells/mm^2 was marked manually for each region.

Nanostring and gene expression analysis

Total RNA was extracted from OCT frozen tissue samples after homogenization using the Qiacube (Qiagen) with the RNeasy kit (cat no. 74106). Quality control for total RNA was performed using the TapeStation 4200 (Agilent) with the RNA kit (cat no. 5067-5576) or RNA HS kit (cat no. 5067-5579). Concentration of the samples was measured with NanoDrop. Using the Nanostring nCounter (Nanostring Technologies), gene expression was conducted for each sample using the Mouse Pan Cancer IO 360 panel that includes 770 gene probes. Each reaction contained 150 ng of total RNA in a 5 μL aliquot, plus reporter and capture probes. The signal quantification was performed by Nanostring digital analyzer, setting the fields of view at 555. Analysis and normalization of the raw Nanostring data was conducted using nSolver (Nanostring Technologies) Advanced Analysis software. Raw counts were normalized to internal levels of reference genes, according to default settings. As recommended by Nanostring, uncertain counts were removed by setting "threshold count value" to 50 and "observation frequency" to 0.9. Gene-set analysis was evaluated by undirected and directed significant scores. Global significance scores (also called undirected significance scores) measure the overall differential expression of the selected gene set relative to selected covariates. Directed global significance scores measure the extent to which a given gene set is up- or downregulated relative to a given covariate. Pathways with undirected scores above 1.5 global significance score were selected.

Gene set enrichment analysis (GSEA)

GSEA analysis was performed on the normalized linear count data file exported from nSolver advanced analysis, that was adjusted to fit the GSEA 4.2.2 input requirements. The analysis was performed according to GSEA recommendations for n = 5/group (permutation type = gene_set and default number of permutation = 1000) using the Chip platform "Mouse_Gene_Symbol_Remapping_Human_Orthologs_MSigDB.v7.5.1.chip." Gene sets were considered significant at false discovery rate (FDR) <25%.

Statistical analysis

Tumor volume over time was assessed and compared between the groups using repeated measured analysis of variance with FDR correction for multiple comparisons. The cubic root transformed volume was modeled as a function of group, day (categorical), and the day X group interaction with baseline volume entered as a covariate. The model estimated means (least squares means) and confidence intervals were estimated from the interaction term and were back transformed to the volume. Each group was analyzed until the time point at which the first animal died. The days for which the differences were significant were mentioned in the result section and the *P* value range was presented. The time required for the tumor to reach 10-fold of its initial size was depicted by a Kaplan-Meier plot; 2 curves are compared with a log-rank test and *P* values adjusted for multiple comparisons were obtained using the FDR method. The above-mentioned analyses were performed using SAS V9.4 (SAS Institute, Cary NC) software. Grubbs's test was used to identify outliers that were removed from the final analysis. To quantify the strength and direction of the relationship between 2 variables, Pearson's linear correlation coefficient r was used, with respective *P* value, for the difference between the means of 2 treatments in ex-vivo (IHC, flow cytometry) studies, a 2-tailed Student's *t* test was used (Excel, Microsoft). *P* value <.05 was considered as a significant difference between the different treatment groups.

Results

DaRT potentiates aPD-1-induced tumor growth retardation in mice bearing SCC tumors

It was hypothesized that DaRT-induced DNA damage and tumor cell death can trigger the activation of an antitumor immune response that eventually potentiates aPD-1 efficacy in SCC tumors. To test this hypothesis, mice bearing SQ2 tumors (~55 mm^3) were treated with aPD-1 therapy using a regimen that shows no efficacy of aPD-1 monotherapy compared with control. It was then examined whether in such settings, a DaRT and aPD-1 combination would be more effective relative to DaRT monotherapy, suggesting an activation of immune-induced tumor cell killing in addition to the direct tumor cell killing induced by alpha radiation. Mice bearing SQ2-derived tumors were treated with a DaRT or inert seed on day 0. In

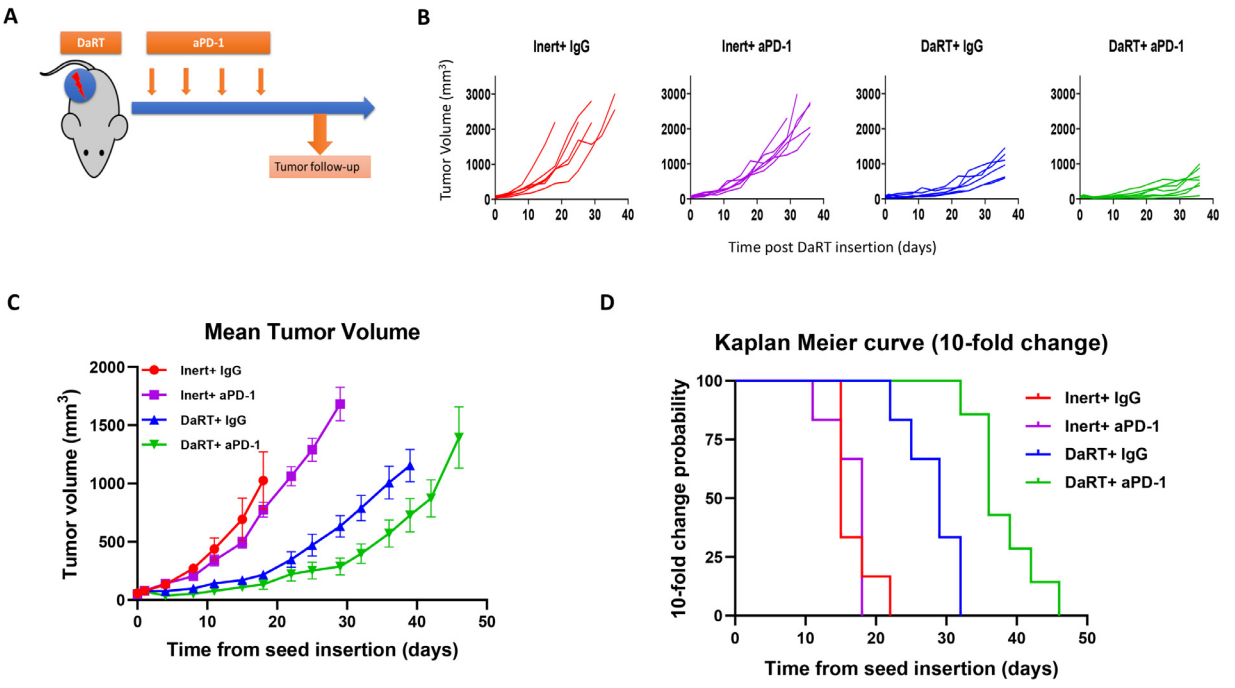

Fig. 1. Combining diffusing alpha-emitters radiation therapy (DaRT) with aPD-1 resulted in a significant reduction in tumor growth compared with monotherapies. (A) Study design. DaRT insertion was performed on day 0, mice were treated with 4 doses of aPD-1 on days 2, 4, 8, and 12. Tumor volume was measured twice a week for tumor growth follow-up. (B) Individual tumor growth for each therapeutic group. (C) Mean tumor volumes ± standard error. aPD-1 was not significantly different from control; DaRT treatment significantly delayed tumor development compared with control or aPD-1 ($P < .05$). The combined treatment (n = 7) enhanced tumor growth retardation relative to control (n = 6) (days 4-18, $P < .05$-.0001), DaRT monotherapy (n = 6) (days 18-39 $P < .05$-.0001) or to aPD-1 alone (n = 6) (days 4-29 $P < .05$-.0001). (D) Tumor growth is significantly delayed in the combination or DaRT groups compared with all other treatments ($P < .005$). No significant difference was observed between aPD-1 and control. Ten-fold tumor volume change probability was calculated by the Kaplan-Meier estimated probability of the time at which the tumors reached 10-times of their initial size, for every time point from the day of DaRT insertion. The inert group showed an average time of 17 days to reach 10-fold of tumor size, aPD-1 16.3 days, DaRT 28.1 days, and DaRT + aPD-1 38.1 days.

addition, 10 mg/kg of aPD-1 or isotype control were injected intraperitoneally on days 2, 4, 8, and 12 (Fig. 1A).

Although no significant effect on tumor growth retardation was observed for aPD-1 therapy (n = 6) relative to control (n = 6), DaRT treatment (n = 6) delayed tumor development compared with control (days 8-18, $P < .05$-.0001) or to aPD-1 (days 4-29, $P < .05$-.0001). The combined treatment enhanced tumor growth retardation relative to control (days 4-18, $P < .05$-.0001), DaRT monotherapy (days 18-39, $P < .05$-.0001) or to aPD-1 alone (days 4-29, $P < .05$-.0001). Tumor retardation induced by the combined treatment reached its peak ~30 days from seed insertion, about 2 weeks after aPD-1 treatment ended and 95% of the total radiation dose was delivered (Fig. 1B, C). The Kaplan-Meier curve (Fig. 1D) showed that while the average length of time required for the tumor to reach 10-fold of its initial size after aPD-1 therapy was not changed relatively to the control, DaRT significantly prolonged this period compared with control or aPD-1 (log-rank test; $P < .005$) and adding aPD-1 to DaRT significantly increased this period relatively to DaRT alone, aPD-1 alone or to control ($P < .005$). The data indicate that aPD-1 exerted an immune mediated tumor cell killing, which is not related to the dispersion of alpha emitting atoms in the tumor. Because such aPD-1 effect was not observed for aPD-1 monotherapy and the combined treatment was more effective than either of the monotherapies, these results might indicate a synergistic or an additive immune-related therapeutic effect of DaRT and aPD-1 combinational treatment.

Combining DaRT and aPD-1 potentiates lymphocyte infiltration and effector function

The above result indicates that DaRT-induced cell death leads to changes in the tumor microenvironment that may be receptive to the activity of cytotoxic lymphocytes under PD-1 blockade and enhance its efficacy, as shown in Fig. 1. To investigate this, mice bearing SQ2 tumors (tumor volume ~48 mm^3) were treated with either DaRT or inert seeds on day 0 in combination with 5 doses of aPD-1 or isotype control (IgG) on days 2, 5, 8, 11, and 14 (Fig. 2A). The effect of DaRT and aPD-1 on T lymphocytes tumor infiltration was assessed 16 days post DaRT insertion (2 days after the

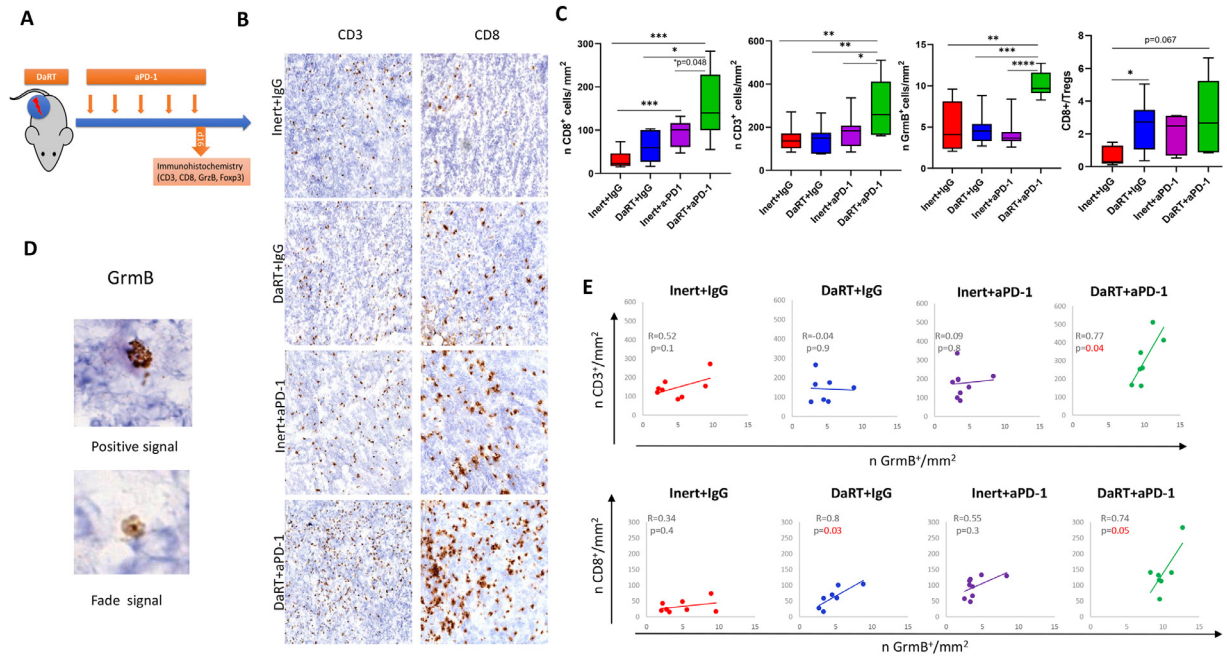

Fig. 2. Diffusing alpha-emitters radiation therapy (DaRT) in combination with aPD-1 therapy induces lymphocyte intratumoral infiltration and granzyme B secretion more than the monotherapies (A) Graphical representation of the experimental design. Mice were treated with 5 doses of aPD-1 in combination with DaRT. Tumors were resected at day 16 and subjected to immunohistochemistry. (B) Representative images of the CD8, CD3 IHC staining in each group (20 × magnification). (C) Box plots showing the number of DAB positive cells per area (mm^2) on immunohistochemically stained tumor tissues for CD3, CD8 (N = 8, N = 7, N = 9, and N = 8), Granzyme B (N = 8, N = 7, N = 9, and N = 7), and CD8/Tregs ratio (N = 5, N = 6, N = 7, and N = 5). "N" denotes the number of samples analyzed in the Inert + IgG, DaRT + IgG, Inert + aPD-1, and DaRT + aPD-1 groups, respectively. (D) Images of Granzyme B staining. The upper panel shows a strong positive signal of Granzyme B granules being secreted by the cell, and the lower panel shows a fade staining that was considered negative in our analysis. (E) Scatter plots (with fitted linear curve) between Granzyme B versus CD3, and Granzyme B versus CD8, R = Pearson's correlation coefficient.

last aPD-1 dose) by immunohistochemical staining of CD3, CD8, Foxp3, and Granzyme B. Notably, several samples were excluded from the IHC analysis of Granzyme B and Foxp3 due to insufficient sections (see number of samples in the legend of Fig. 2). The results represent the cumulative data of 2 independent experiments.

The results demonstrated a significant increase in the density of CD3+ or CD8+ cells in the combination group relative to control or to monotherapies ($P < .05$; Fig. 2B, C). aPD-1 monotherapy induced CD8+ infiltration to the tumor, yet in a significantly lower extent relative to the combinational treatment ($P < .05$). Moreover, whereas aPD-1 or DaRT monotherapies were not accompanied by an increase in granzyme B release, a significant increase was observed in the combinational therapy (Fig. 2C, D). Furthermore, the CD8/Tregs ratio was increased in DaRT group compared with control ($P < .05$) and a similar trend ($P = .067$) was observed for the combination group. Because granzyme B release is also mediated by other effector cells, such as NK, the extent of granzyme B positive signal was correlated with CD3+ and CD8+ densities in the tumor. It was found that CD3+ density is positively correlated with granzyme B only in the combined treatment. In addition, CD8+ density was positively correlated with granzyme B only in the combined or DaRT treatments (Fig. 2E).

DaRT in combination with aPD-1 reduces tumoral general MDSC and splenic PMN-MDSCs populations compared with aPD-1 monotherapy

To investigate possible systemic implications of the combined treatment, flow cytometry analyses of MDSCs and activated DCs (aDCs) populations in the spleen and in the tumor were performed at day 16, when the combined treatment showed a synergistic effect on TILs densities (Fig. 3A). Notably, one animal in the DaRT group was not included in the tumor flow analysis due to insufficient number of cells. The results represent the cumulative data of 2 independent experiments.

The analysis showed that the general MDSCs population in the tumor was reduced in DaRT or in the combinational treatment, compared with aPD-1 treatment (Fig. 3B). In the spleen, the general MDSCs population was reduced in the DaRT group compared with the control but not in the

combination. All treatment groups presented a reduced percentage of PMN-MDSCs in the spleen compared with inert control. Yet, the combinational treatment led to a significantly higher reduction of this population in the spleen compared with aPD-1 monotherapy. The splenic M-MDCS subpopulation correlated with the splenic aDCs population, only for DaRT treatment (Fig. 3C), suggesting a possible functional relation between the 2 populations in response to DaRT.

DaRT activates intratumoral DCs, in correlation with splenic aDCs, and induces MDSCs distribution changes both locally and peripherally

To investigate the potential mechanisms underlying the effects observed in the previous results, DaRT-induced "early" changes in the tumor microenvironment were characterized 7 days post seed insertion (Fig. 4A), using 2 approaches: (1) immune phenotyping and (2) gene expression. SQ2-bearing mice (tumor volume ~85 mm^3; n = 5, per group) were treated with DaRT or inert seeds (day 0) and 2 doses of IgG antibody (days 2, 5). Seven days post seed insertion tumors and spleens were harvested and subjected to flow cytometry analysis, and the mRNA extracted from these tumors was used for NanoString analysis.

The flow cytometry analysis revealed an increase in the percentage of aDCs in DaRT-treated tumors while the proportion of total intratumoral DCs remained unchanged (Fig. 4B, C). Activated DCs in the tumor positively correlated with aDCs in the spleen for DaRT-treated mice (Fig. 4D, upper panel) and with M-MDSCs in the tumor (Fig. 4D, lower panel). An increase in the percentage of M-MDSCs in the tumor and a decrease of the same population in the spleen were detected (Fig. 4E, F, lower panels). On the contrary, PMN-MDSCs were found to be increased in the spleen and did not show significant change in the tumor (Fig. 4E).

Differential gene expression analysis identifies the induction of apoptotic, interferon signaling, and myeloid compartment related gene expression in response to DaRT

To investigate pathways activated by DaRT, the mRNA extracted from DaRT- or inert- treated tumors (the same tumors as described in the previous result) was analyzed using Nanostring PanCancer IO360 panel 7 days post seed insertion (Fig. 5A). Differential gene expression analysis

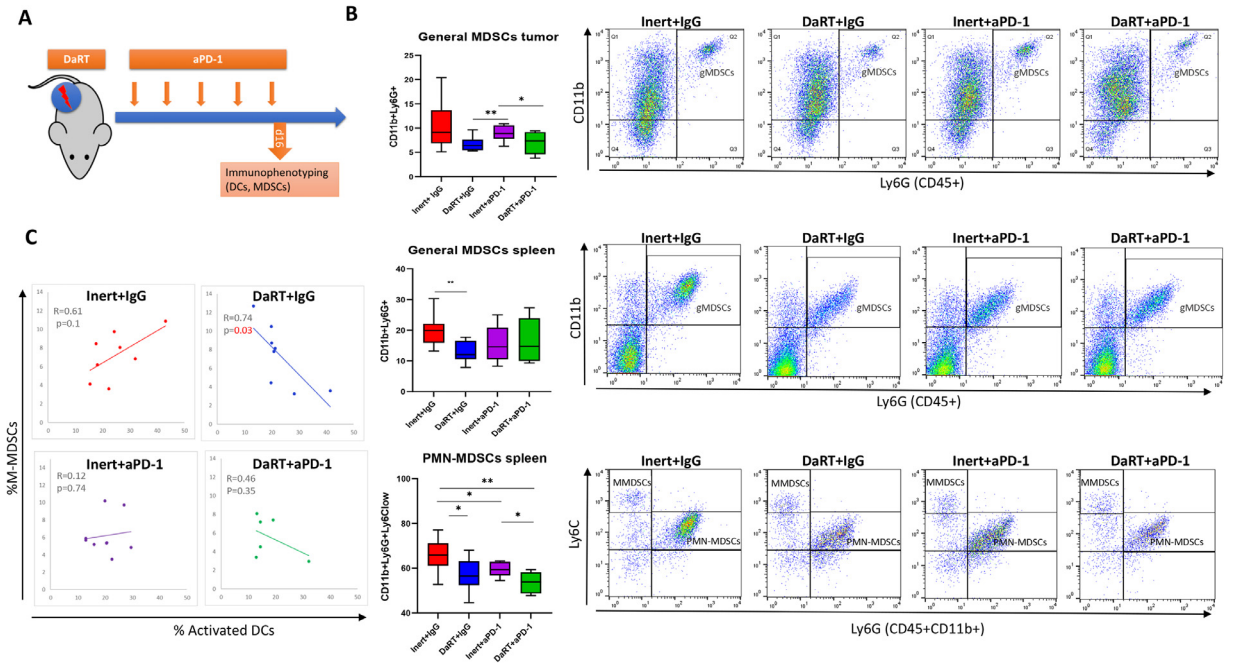

Fig. 3. Peripheral myeloid derived suppressor cells (MDSCs) in response to diffusing alpha-emitters radiation therapy (DaRT) aPD-1 or the combinational treatment. (A) Experimental design. After 5 doses of aPD-1, at day 16 from DaRT insertion tumors and spleens were collected for flow cytometry analysis (FACS). (B) Flow cytometry analysis targeting MDSCs after 16 days from DaRT insertion. N = 8, N = 7, N = 9, and N = 7 tumors, and N = 8, N = 8, N = 9, and N = 6 spleens were analyzed. "N" denotes the number of samples analyzed in the Inert + IgG, DaRT + IgG, Inert + aPD-1, and DaRT + aPD-1 groups, respectively. Polymorphonuclear-MDSCs were gated as CD45+, CD11b+, Ly6G+Ly6C low, and general MDSCs as CD45+, CD11b+ Ly6G+. (C) Negative correlation between splenic M-MDSCs and activated DCs was shown (P = .03) only in the DaRT treated group.

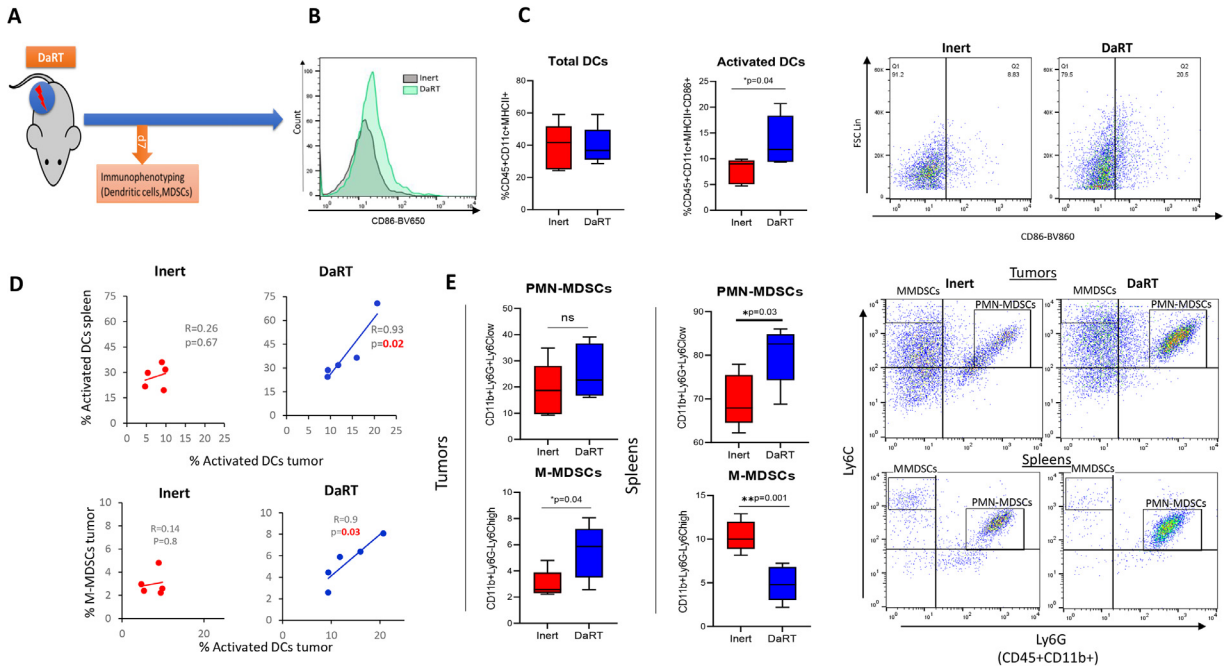

Fig. 4. Diffusing alpha-emitters radiation therapy (DaRT) treatment results in an early intratumoral dendritic cells (DCs) activation that positively correlates with DCs activation in the spleen and myeloid derived suppressor cells (MDSCs) distribution changes. (A) Graphical representation of the experimental design. Tumors were collected for flow cytometry analysis 7 days post-DaRT insertion. n = 5 for each group. (B) Histogram representing the shift in aDCs counts after DaRT treatment. (C) Flow cytometry analysis shows a significant increase in tumoral activated DCs in DaRT versus Inert (right panels) despite the similar number of DCs detected in both groups (left panels). DCs were gated on CD45+, CD11c+, MHCII+ cells, and CD86 was used as an activation marker. (D) Linear regression analysis shows a significant positive correlation between the percentage of activated DCs in the tumor with those in the spleen (r = 0.93 P = .02) in DaRT treated tumors. (E) Box plots and representative flow cytometry analysis in the spleen and tumor of DaRT treated mice showing a slight increase in PMN-MDSCs (not significant) (upper left panel) and a significant increase in M-MDSCs ($P < .05$) (lower left panel) in DaRT treated tumors. In the spleens, an increase in PMN-MDSCs ($P < .05$) and a decrease in M-MDSCs ($P < .005$) was detected. PMN-MDSCs were identified as CD45+, CD11b+Ly6G+Ly6C^{low}, and Monocytic MDSCs were gated on CD45+, CD11b+Ly6G^{-}, Ly6C^{high}. *Abbreviations*: DaRT = DaRT + IgG; Inert = Inert + IgG.

(Fig. 5B, Supplementary File 2, Table S1) identified genes that were significantly differentially expressed ($P < .05$). Among the top upregulated are genes involved in apoptosis and G1/S cell cycle arrest, such as *BAX, CASP1, MDM2, E3F3,* and *CDKN1A* (p21). In addition, inflammatory cytokines such as *CXCl2/3* and *TNFSF4* (OX-40), interferon signaling related genes such as *IFIT1* and *RSAD2,* and antigen presentation related genes such as *H2-K1* (murine MHC class 1) and *CTSS,* were upregulated. Genes related to DNA repair such as *FANCA* and *POLD1,* and to Notch signaling such as *HEY1, MFNG,* were downregulated. *CD244* that mediates non-MHC restricted NK/T cell killing[33] and *KLRD1* (CD94), *ULBP1* (NKG2D ligand) were downregulated, together with TCR- signaling related genes *CD247* (CD3 zeta) and *ZAP70.*

Gene-set analysis highlighted pathways (undirected global significance score >1.5) that are potentially involved in the tumor response to DaRT treatment (Fig. 5C, Supplementary File 2, Table S2). The directed global significance scores identified apoptosis, myeloid-compartment, and interferon signaling as positively changed pathways, while notch signaling, DNA damage repair, cell proliferation, epigenetic regulation, and angiogenesis were negatively scored (Fig. 5C). Other processes such as antigen presentation, chemokines and cytokines, metabolic stress, and NF-kappaB signaling showed high undirected global score (US > 1.5) with low directional score ($-1 < DS < 1$). Cell type profiling analysis (Fig. 5D) demonstrates an increase in transcription related to phagocytes such as macrophages and neutrophils and a potential decrease in exhausted CD8, Tregs and cytotoxic cells related transcription (Fig. 5D). Corresponding with the above results, the Pathway Scoring module showed an increase in mitochondrial-related apoptosis, myeloid compartment, and chemokines/cytokines signaling, and a decrease in cell proliferation, notch signaling, and lymphoid compartment (Fig. 5E). NanoString counts were validated by IHC staining of foxp3 in the tumor (Supplementary File 1, Fig. S2). This test showed high correlation between the IHC staining and RNA counts (r = 96, $P < .00005$).

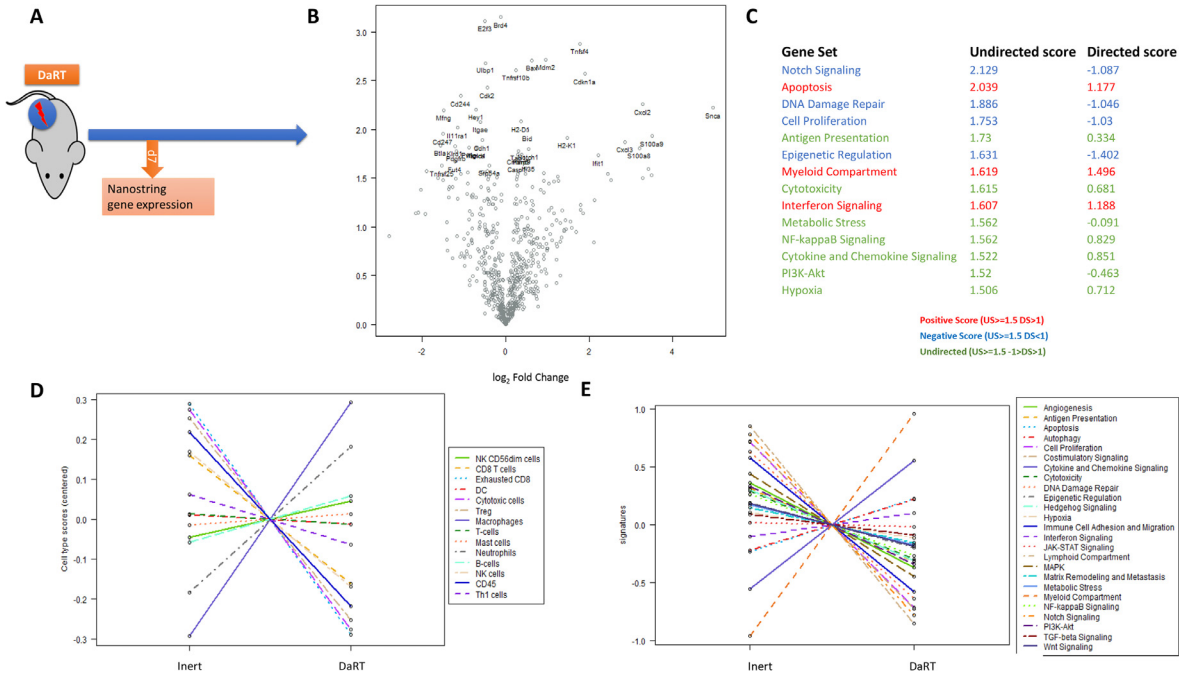

Fig. 5. Gene expression analysis based on Nanostring PanCancer IO360 panel using mRNA isolated from SQ2 tumors after diffusing alpha-emitters radiation therapy (DaRT) treatment. (A) Study design. DaRT or inert treated tumors (n = 5) were harvested 7 days post seed insertion and were subjected to gene expression analysis. (B) Volcano plot displays genes according to their $\log_2$fold change and $-\log_{10}P$ value (x and y axes, respectively). Top differentially expressed (DE) targets are labeled. (C) Global significant score table. List of possible differentially expressed pathways according to undirected (US) and directed (DS) global scores. US measures the overall differential expression of the selected gene set, ignoring whether each gene is up- or downregulated, while DS measures the extent to which a given gene set is up- or downregulated in response to the treatment. Red = positive score (US >1.5 and DS >1); blue = negative score (US >1.5 and DS < −1); green = uncertain direction pathways with (US >1.5, −1 < DS < 1). (D) Cell type profiling showing the raw level of abundance of potential cell populations for each treatment. (E) "Pathway score" among DaRT treated versus untreated tumors. Lines show each pathway's average score across values of Treatment. *Abbreviations:* *"DaRT" = DaRT + IgG; "Inert" = Inert + IgG.

Gene set enrichment analysis identifies p53, TNF-alpha, IFN-alpha, IFN-gamma, and mTOR1-related signaling in DaRT phenotype

To validate these results and gain additional insight, a GSEA analysis, which determines whether a priori-defined set of genes shows significant concordant differences between 2 biological states (DaRT vs. Inert), was performed on the normalized linear mRNA counts (Supplementary File 2, Table S3). The analysis highlighted a set of genes that were similar to those identified by the gene expression analysis of nSolver above (including top ranked genes like *MDM2, BAX, TNFSF4*, and more; Fig. 6A). Running GSEA against the "hallmark" database identified upregulated gene sets in DaRT phenotype, among them 11 gene sets were significant (FDR <25%), including: TNF-alpha signaling via NF-KB, P53 pathway, mTORC1 complex signaling, upregulated UV response, IFN alpha and IFN gamma signaling, complement, IL-6/JAK/STAT3 signaling, hypoxia, glycolysis, and apoptosis (Fig. 6A, upper panel). Nine gene sets were upregulated among inert phenotype including ETM transition, STAT5 in response to IL2 stimulation, down regulation of UV response, and E2F targets, yet only one gene set, the G2/M checkpoint, was at FDR <25% (Fig. 6A, lower panel). Running GSEA against the "Reactome" databases, identified 55 additional gene sets that are upregulated in DaRT phenotype, among them 15 gene sets were significant (FDR <25%). These included neutrophils degranulation, antigen presentation, TLR signaling, IL-1/IL-10 signaling, chemokines, and innate immune system. Fifty-seven gene sets were upregulated in phenotype "Inert," 5 at FDR <25%. Top gene sets were related to DNA DSB repair and homologues recombination (HR) repair, mitotic cell cycle phase, and CD28 costimulation. "KEGG" database identified non-significant tendency to upregulate intracellular pathogen sensing and B cell related pathways in DaRT phenotype (Supplementary File 3).

Discussion

Diffusing alpha-emitters radiation therapy releases alpha-emitting atoms from a Radium-244 loaded seed that gradually spread in the tumor microenvironment,[27] thereby accumulating DNA damage,[22] and killing tumor cells.[21] Gene

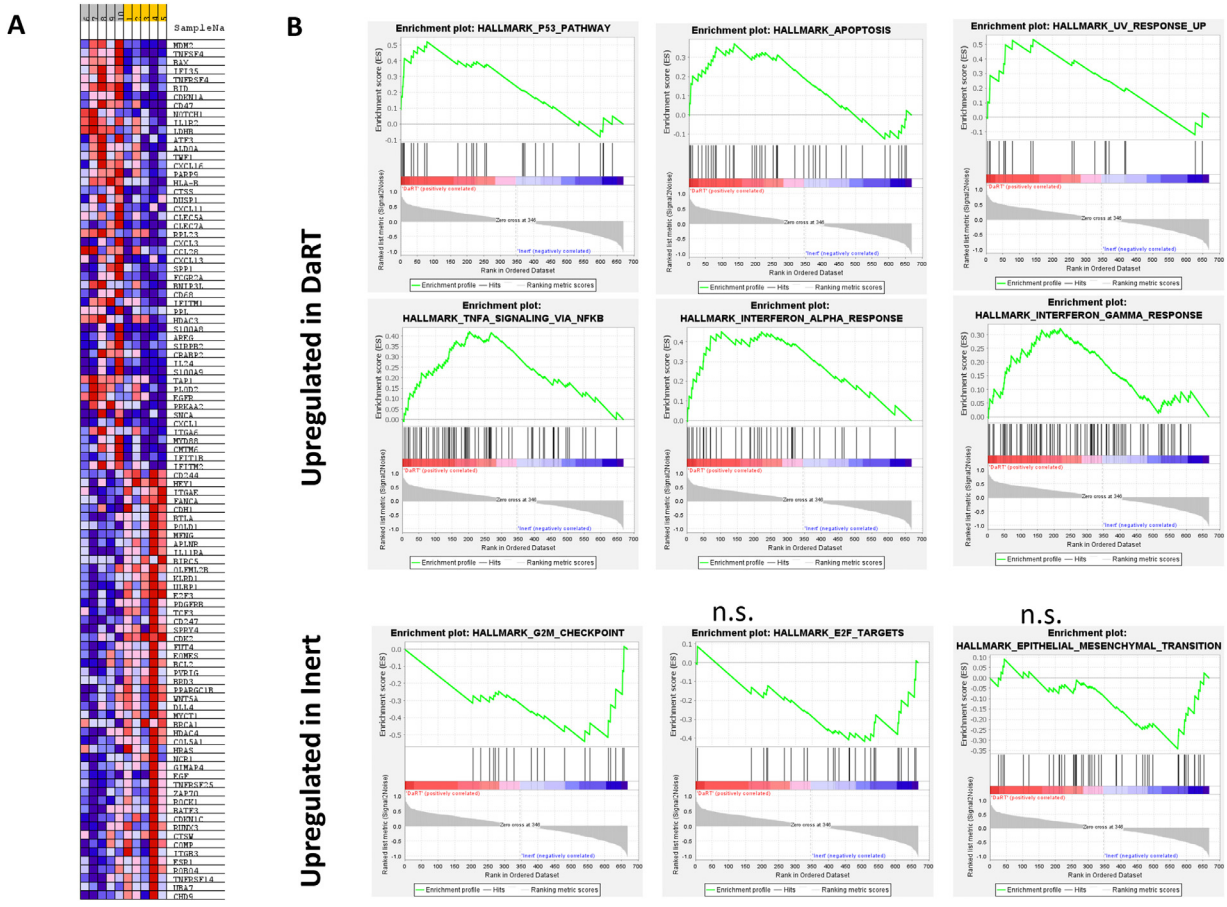

Fig. 6. Gene set enrichment analysis based on Nanostring mRNA normalized counts performed against the "hallmark" gene set database. (A) Selected gene sets upregulated in diffusing alpha-emitters radiation therapy (DaRT) or Inert phenotypes. For each gene set the profile of the running enrichment score (ES) score and positions of GeneSet members on the rank observed list is plotted. (B) Heat map of the top 50 features for each phenotype in ranked gene list correlation profile. Orange-marked columns denote Inert samples, while gray-marked samples denote DaRT samples. Blue and red scales represent gene expression level, where red color refers to high expression and blue color refers to low expression. *Abbreviations:* DaRT = DaRT + IgG; Inert = Inert + IgG.

expression analysis 7 days post DaRT seed insertion revealed that DaRT activates Bax-related mitochondrial apoptosis pathway, p53 signaling, reduced transcription related to proliferation, upregulation of p21 gene expression, and reduced transcription related to G1/S transition. In agreement with this, DaRT also reduced DNA repair transcription, presumably due to unrepairable damage to the DNA and due to G1/S arrest that halts DNA synthesis, which is required for critical DSBs repair pathways such as HR. The focus of the present study was to investigate the implications of such a unique type of radiation therapy, which is distinct from other radiation types in its biological efficiency, place and time, and the type of DNA lesions, on immune-related changes. In addition, to examine whether this type of damage promotes a "hot" tumor microenvironment that eventually will increase responsiveness to aPD-1 therapy.

The gene expression profile of DaRT-treated tumors a week post seed insertion revealed a unique immune state, in which on the one hand transcription related to innate proinflammatory responses, such as interferon signaling, antigen presentation, pathogen recognition, phagocytes recruitment, and chemokines/cytokines release are observed, and on the other hand, reduced transcription related to lymphoid compartment, NK, exhausted T cells, Tregs, but also TCR signaling is observed. The transcription profile at this early time point indicates that DaRT-induced DNA damage releases signals similar to those of response to a viral attack, such as interferon alpha signaling that is activated in response to abnormal double stranded DNA,[34,35] and the antiviral interferon gamma signaling that are known to activate macrophages and neutrophils.[36] Yet, at the same time, cytotoxic related transcription is restrained and indications for a reduction in NK and TCR signaling related gene expression was detected, as indicated by the downregulation of genes like *CD244, KLRD1, NCR1, ZAP70,* and *CD247.*

This state may represent an early time point in which cytotoxic responses are regulated to prevent uncontrolled

response against self-antigens that are released from the dying/dead cells after radiation. The reduction in cytotoxic-related transcription may also agree with the temporarily elevation of M-MDSCs in the tumor suggesting this population as a potential target for therapy with DaRT. In addition, the reduction in T lymphocytes-related transcription may be affected by the upregulation of IL24 that weakens the initial CD8 cell expansion to prevent uncontrolled T cell responses[37] or by decreased notch signaling that is required for T cell differentiation.[38] Downregulation of NK related transcription at this time point may relate to the upregulation of MHC class 1 molecules observed after DaRT treatment.[39]

The increase of M-MDSCs population correlated with aDCs in the tumor, indicating a possible crosstalk between the 2 populations. aDCs in the tumor positively correlated with aDCs in the spleen for DaRT- but not inert-treated mice, indicating the involvement of circulating aDCs in DaRT-induced immune response. This may support a higher potential of tumor antigens recognition by DCs after intratumoral alpha radiation, reflected systematically as well. The overexpression of S100-fammily alarmins (DAMPs)[40] and cd68 macrophage marker[41] supports the induction of phagocytosis, clearance of cells debris and the recruitment and activation of APCs by DaRT. This state is accompanied by transcription of inflammatory cytokines and chemokines such as ccl3, cxcl11, cxcl2/3 that attract immune cells into the tumor.[42] Activation of TLR-related pathways may promote DCs activation observed in flow cytometry and the elevation of genes related to APCs MHC-II antigen presentation such as cathepsin-s.[43,44] An upregulation of OX-40 ligand and receptor, that is involved in T cell APC interactions and mediates adhesion of activated T cells to endothelial cells[45,46] may indicate that a specific immune response is yet to come at a later time point.

In a recent study it was shown that other types of high-LET irradiation (eg, carbon ion radiation therapy) led to the enrichment of similar pathways after treatment.[47] The authors demonstrated enrichment of DNA damage repair pathway several hours after treatment and showed that the prolonged DNA repair period after high LET radiation was linked to an amplified p53 signaling and immune stimulation. Because in the present study the gene expression analysis was performed 1 week after the treatment started and because DaRT treatment is continuous and gradual, our result might represent a later phase of the DNA damage response, in which DNA repair and proliferation are halted, yet the inflammatory response such as expression of cytokines and chemokines can be detected.

When DaRT was combined with aPD-1 and investigated in a later time point (at the time both treatments ended, 16 days after treatment start), aPD-1 monotherapy increased the density of CD8+ T-cells in the tumor; however, no therapeutic effect or elevation in granzyme B secretion was observed. DaRT in combination with aPD-1, potentiated the increase of granzyme B secretion and further elevated CD8+ cells infiltration to the tumor. This result suggests a synergy between the treatments and should be further investigated to rule out an additive effect. Notably, at this time point most of the alpha emitting atoms released from DaRT seeds already decay. This may optimize the timing and conditions of the combination and allow T cell infiltration and function after alpha-induced stimulation.

DaRT as monotherapy, increased CD8+/Tregs ratio in the tumor and led to the reduction of total MDSCs and PMN-MDSCs in the spleen at day 16 post seed insertion. Additionally, DaRT + aPD-1 further reduced splenic PMN-MDSCs compared aPD-1 alone. Because peripheral MDSCs are correlated with prognosis and response to checkpoint blockage[48] this result supports a possible therapeutic advantage in the use of both therapies together. Such a systemic decrease in MDSCs may lead to the potentiation of T cell function at distant sites as well,[49] an important subject for further investigation. It may be suggested that such studies will explore the link between RT regimens, which show similar reduction in MDCSs[49,50] and adaptive immunity activation versus those that fail in doing so. In addition, further investigation may include the activation of STING signaling that is known to decrease MDSCs in the spleen and tumor and to promote adaptive immune responses upon radiation.[9]

Conclusion

DaRT is currently being tested in combination with aPD-1 therapy in mHNSCC patients (NCT05047094). The present study provides an initial insight of the early effect of DaRT-induced DNA damage and provides preclinical evidence for the potentiation of aPD-1 blockade by DaRT that may have important clinical implications for DaRT or aPD-1 treated SCC patients.

References

1. Sharma P, Allison JP. The future of immune checkpoint therapy. *Science* 2015;348:56–61.
2. Marin-Acevedo JA, Dholaria B, Soyano AE, Knutson KL, Chumsri S, Lou Y. Next generation of immune checkpoint therapy in cancer: new developments and challenges. *J Hematol Oncol* 2018;11:39.
3. Ostrand-Rosenberg S, Horn LA, Haile ST. The programmed death-1 immune-suppressive pathway: Barrier to antitumor immunity. *J Immunol* 2014;193:3835–3841.
4. Nowicki TS, Hu-Lieskovan S, Ribas A. Mechanisms of resistance to PD-1 and PD-L1 blockade. *Cancer J* 2018;24:47–53.
5. Yi M, Zheng X, Niu M, Zhu S, Ge H, Wu K. Combination strategies with PD-1/PD-L1 blockade: Current advances and future directions. *Mol Cancer* 2022;21:28.
6. Aznar MA, Tinari N, Rullán AJ, et al. Intratumoral delivery of immunotherapy-act locally, think globally. *J Immunol* 2017;198:31–39.
7. Galluzzi L, Buqué A, Kepp O, Zitvogel L, Kroemer G. Immunogenic cell death in cancer and infectious disease. *Nat Rev Immunol* 2017;17:97–111.

8. Storozynsky Q, Hitt MM. The impact of radiation-induced dna damage on cGAS-STING-mediated immune responses to cancer. *Int J Mol Sci* 2020;21:8877.
9. Deng L, Liang H, Xy M, et al. STING-dependent cytosolic DNA sensing promotes radiation-induced type I interferon-dependent antitumor immunity in immunogenic tumors. *Immunity* 2014;41:843–852.
10. Pardoll DM. The blockade of immune checkpoints in cancer immunotherapy. *Nat Rev Cancer* 2012;12:252–264.
11. Yin L, Xue J, Li R, et al. Effect of low-dose radiation therapy on abscopal responses to hypofractionated radiation therapy and anti-PD1 in mice and patients with non-small cell lung cancer. *Int J Radiat Oncol Biol Phys* 2020;108:212–224.
12. Lee YH, Tai D, Yip C, Choo SP, Chew V. Combinational immunotherapy for hepatocellular carcinoma: Radiotherapy, immune checkpoint blockade and beyond. *Front Immunol* 2020;11 568759.
13. Chen L, Douglass J, Kleinberg L, et al. Concurrent immune checkpoint inhibitors and stereotactic radiosurgery for brain metastases in non-small cell lung cancer, melanoma, and renal cell carcinoma. *Int J Radiat Oncol Biol Phys* 2018;100:916–925.
14. Roger A, Finet A, Boru B, et al. Efficacy of combined hypo-fractionated radiotherapy and anti-PD-1 monotherapy in difficult-to-treat advanced melanoma patients. *Oncoimmunology* 2018;7 e1442166.
15. Yilmaz MT, Elmali A, Yazici G. Abscopal effect, from myth to reality: From radiation oncologists' perspective. *Cureus* 2019;11:e3860.
16. Sharabi AB, Nirschl C, Kochel CM, et al. Stereotactic radiation therapy augments antigen-specific PD-1-mediated antitumor immune responses via cross-presentation of tumor antigen. *Cancer Immunol Res* 2015;3:345–355.
17. Kiang JG, Olabisi AO. Radiation: A poly-traumatic hit leading to multi-organ injury. *Cell Biosci* 2019;9:25.
18. Popovtzer A, Rosenfeld E, Mizrachi A, et al. Initial safety and tumor control results from a "first-in-human" multicenter prospective trial evaluating a novel alpha-emitting radionuclide for the treatment of locally advanced recurrent squamous cell carcinomas of the skin and head and neck. *Int J Radiat Oncol Biol Phys* 2020;106:571–578.
19. Bellia SR, Feliciani G, Del Duca M, et al. Clinical evidence of abscopal effect in cutaneous squamous cell carcinoma treated with diffusing alpha emitters radiation therapy: A case report. *J Contemp Brachytherapy* 2019;11:449–457.
20. Cooks T, Arazi L, Schmidt M, et al. Growth retardation and destruction of experimental squamous cell carcinoma by interstitial radioactive wires releasing diffusing alpha-emitting atoms. *Int J Cancer* 2008;122:1657–1664.
21. Arazi L, Cooks T, Schmidt M, Keisari Y, Kelson I. Treatment of solid tumors by interstitial release of recoiling short-lived alpha emitters. *Phys Med Biol* 2007;52:5025–5042.
22. Franken NA, Hovingh S, Ten Cate R, et al. Relative biological effectiveness of high linear energy transfer alpha-particles for the induction of DNA-double-strand breaks, chromosome aberrations and reproductive cell death in SW-1573 lung tumour cells. *Oncol Rep* 2012;27:769–774.
23. Hada M, Georgakilas AG. Formation of clustered DNA damage after high-LET irradiation: A review. *J Radiat Res* 2008;49:203–210.
24. Hodgkins PS, O'Neil P, Stevens D, Fairman MP. The severity of alpha-particle-induced DNA damage is revealed by exposure to cell-free extracts. *Radiat Res* 1996;146:660–667.
25. Roobol SJ, van den Bent I, van Cappellen WA, et al. Comparison of high- and low-LET radiation-induced DNA double-strand break processing in living cells. *Int J Mol Sci* 2020;21:6602.
26. Nickoloff JA, Sharma N, Taylor L. Clustered DNA double-strand breaks: Biological effects and relevance to cancer radiotherapy. *Genes (Basel)* 2020;11:99.
27. Arazi L. Diffusing alpha-emitters radiation therapy: Approximate modeling of the macroscopic alpha particle dose of a point source. *Phys Med Biol* 2020;65 015015.
28. Confino H, Hochman I, Efrati M, et al. Tumor ablation by intratumoral Ra-224-loaded wires induces anti-tumor immunity against experimental metastatic tumors. *Cancer Immunol Immunother* 2015;64:191–199.
29. Confino H, Schmidt M, Efrati M, et al. Inhibition of mouse breast adenocarcinoma growth by ablation with intratumoral alpha-irradiation combined with inhibitors of immunosuppression and CpG. *Cancer Immunol Immunother* 2016;65:1149–1158.
30. Domankevich V, Cohen A, Efrati M, et al. Combining alpha radiation-based brachytherapy with immunomodulators promotes complete tumor regression in mice via tumor-specific long-term immune response. *Cancer Immunol Immunother* 2019;68:1949–1958.
31. Domankevich V, Efrati M, Schmidt M, et al. RIG-1-like receptor activation synergizes with intratumoral alpha radiation to induce pancreatic tumor rejection, triple-negative breast metastases clearance, and antitumor immune memory in mice. *Front Oncol* 2020;10:990.
32. Blank M, Mandel M, Hazan S, Keisari Y, Lavie G. Anti-cancer activities of hypericin in the dark. *Photochem Photobiol* 2001;74:120–125.
33. Agresta L, Hoebe KHN, Janssen EM. The emerging role of CD244 signaling in immune cells of the tumor microenvironment. *Front Immunol* 2018;9:2809.
34. Katashiba Y, Miyamoto R, Hyo A, et al. Interferon-alpha and interleukin-12 are induced, respectively, by double-stranded DNA and single-stranded RNA in human myeloid dendritic cells. *Immunology* 2011;132:165–173.
35. Sausen DG, Reed KM, Bhutta MS, Gallo ES, Borenstein R. Evasion of the host immune response by betaherpesviruses. *Int J Mol Sci* 2021;22:7503.
36. Tau G, Rothman P. Biologic functions of the IFN-gamma receptors. *Allergy* 1999;54:1233–1251.
37. Persaud L, De Jesus D, Brannigan O, et al. Mechanism of action and applications of interleukin 24 in immunotherapy. *Int J Mol Sci* 2016;17:869.
38. Kelliher MA, Roderick JE. NOTCH signaling in T-Cell-mediated anti-tumor immunity and T-cell-based immunotherapies. *Front Immunol* 2018;9:1718.
39. Herzer K, Falk CS, Encke J, et al. Upregulation of major histocompatibility complex class I on liver cells by hepatitis C virus core protein via p53 and TAP1 impairs natural killer cell cytotoxicity. *J Virol* 2003;77:8299–8309.
40. Christmann C, Zenker S, Marten L, et al. Interleukin 17 promotes expression of alarmins S100A8 and S100A9 during the inflammatory response of keratinocytes. *Front Immunol* 2020;11 599947.
41. Chistiakov DA, Killingsworth MC, Myasoedova VA, et al. CD68/macrosialin: Not just a histochemical marker. *Lab Invest* 2017;97:4–13.
42. Vilgelm AE, Richmond A. Chemokines modulate immune surveillance in tumorigenesis, metastasis, and response to immunotherapy. *Front Immunol* 2019;10:333.
43. Riese RJ, Wolf PR, Brömme D, et al. Essential role for cathepsin S in MHC class II-associated invariant chain processing and peptide loading. *Immunity* 1996;4:357–366.
44. Conus S, Simon HU. Cathepsins and their involvement in immune responses. *Swiss Med Wkly* 2010;140:w13042.
45. Imura A, Imura A, Hori T, Imada K, et al. The human OX40/gp34 system directly mediates adhesion of activated T cells to vascular endothelial cells. *J Exp Med* 1996;183:2185–2195.
46. Fu Y, Lin Q, Zhang Z, Zhang L. Therapeutic strategies for the costimulatory molecule OX40 in T-cell-mediated immunity. *Acta Pharm Sin B* 2020;10:414–433.
47. Macaeva E, Tabury K, Michaux A, et al. High-LET carbon and iron ions elicit a prolonged and amplified p53 signaling and inflammatory response compared to low-LET X-rays in human peripheral blood mononuclear cells. *Front Oncol* 2021;11 768493.
48. Peranzoni E, Ingangi V, Masetto E, Pinton L, Marigo I. Myeloid cells as clinical biomarkers for immune checkpoint blockade. *Front Immunol* 2020;11:1590.
49. Lan J, Li R, Yin L-M, et al. Targeting myeloid-derived suppressor cells and programmed death ligand 1 confers therapeutic advantage of ablative hypofractionated radiation therapy compared with conventional fractionated radiation therapy. *Int J Radiat Oncol Biol Phys* 2018;101:74–87.
50. Zhou H, Yang P, Li H, et al. Carbon ion radiotherapy boosts anti-tumour immune responses by inhibiting myeloid-derived suppressor cells in melanoma-bearing mice. *Cell Death Discov* 2021;7:332.